

# Corrosion of Structural Ceramics Under Sub-Critical Conditions in Aqueous Sodium Chloride Solution and in Deionized Water. Part II: Dissolution of Al<sub>2</sub>O<sub>3</sub>-Based Ceramics

Dagmar Galusková†

Vitrum Laugaricio – Joint Glass Center of the IIC SAS, TnU AD, FChFT STU and RONA j.s.c.,  
Trenčín 911 50, Slovakia

Miroslav Hnatko, Dušan Galusek,\* and Pavol Šajgalík\*

Institute of Inorganic Chemistry, Slovak Academy of Sciences, Bratislava 845 36, Slovakia

Two types of alumina-based ceramics, pure solid-state sintered (SSS) alumina ceramics, and a liquid phase sintered (LPS) alumina were corrosion tested under both static and quasi-dynamic conditions in 0.5M NaCl solution and in deionized water reference medium at the temperature of 290°C. Static tests were also performed at 150° and 200°C in order to obtain the data for determination of kinetic parameters, and for calculation of the activation energies. The apparent activation energies of dissolution of the LPS alumina in deionized water and in 0.5M NaCl solution were identical and ranged around 49 kJ/mol. The SSS alumina ceramics corroded by grain-boundary attack and slow dissolution of alumina matrix grains, and the corrosion rates were negligible in both corrosion media. The LPS alumina, corroded by preferential attack and dissolution of calcium aluminosilicate grain-boundary glass. The alumina matrix remained relatively intact. The dissolution was markedly faster than in the SSS alumina. The rates of dissolution were found to be temperature dependent, but no influence of the corrosion medium was observed.

## I. Introduction

CORROSION of nonoxide ceramics in contact with aqueous solutions under subcritical conditions was discussed in detail in Part I of this paper. The chemical resistance of the ceramics based on Si<sub>3</sub>N<sub>4</sub> was found to be relatively low and not sufficient for applied conditions and corrosion environment.<sup>1</sup> Generally, there exist significant differences in the mechanisms of corrosion and the corrosion resistance of different groups of ceramic materials (silicate, oxide, and nonoxide ceramic). The chemical composition and microstructure are the key factors in terms of their corrosion resistance.

The papers dealing with corrosion resistance of alumina ceramics report on the corrosion in aqueous acidic<sup>2,3</sup> or caustic<sup>4,5</sup> solutions at high temperatures. The corrosive effect of the acids on alumina ceramics decreases in the order H<sub>3</sub>PO<sub>4</sub> > HCl > H<sub>2</sub>SO<sub>4</sub>, where the dominant corrosion mechanisms were identified as intergranular attack and dissolution of Al<sub>2</sub>O<sub>3</sub>.<sup>6</sup> Whether alumina could be prone to corrosion also in neutral aqueous environments remains questionable, and to our knowledge has

not been studied by any research group working in the area of corrosion of structural ceramics.

A related area, not covered in this study, is supercritical water oxidation (SCWO): high-temperature and supercritical water provide promising environment for various processes, e.g. chemical reactions, salt separation processes, oxidation of organic wastes, etc. Known for its extreme corrosiveness the SCWO unite represent a significant challenge for material selection: no material can withstand every conceivable acidic high-temperature solution. On the other hand, some materials possess a good corrosion resistance in the absence of some species,<sup>7</sup> thus giving a chance for tailoring materials for specific needs.

Alumina is generally considered as an appropriate, and particularly from the economical point of view, suitable ceramics for such oxidizing corrosion environments. To understand mechanisms of degradation in more complex systems, model experiments were carried out with simpler systems, where aggressive acidic and caustic conditions were avoided at the very beginning of the dissolution process. The corrosion experiments under static and so called quasi-dynamic conditions were performed in deionized water and in the 0.5M NaCl solution with neutral pH at temperatures ≤290°C. For evaluation of the corrosion mechanisms the emphasis was put on determination of the eluate chemistry combined with the chemical and phase analysis of formed corrosion products. The effect of additives on corrosion resistance of the liquid phase sintered (LPS) alumina was evaluated and compared to high purity solid-state sintered (SSS) alumina.

## II. Experimental Procedure

### (1) Materials Characterization

Both tested aluminas were prepared from ultra fine (particle size 150 nm) and ultra pure (99.995 wt%) alumina powder Taimicron TM DAR (Taimei Ltd., Tokyo, Japan). The pure SSS alumina (material A) was prepared by sintering of slip cast green bodies at 1350°C for 1 h, achieving the relative density of 99.8%. LPS-sintered alumina was prepared by hot pressing at 1450°C and 20 MPa of the same powder containing 5 wt% of CaO · 5SiO<sub>2</sub> sintering additives (material AH), achieving the relative density 99.2%.

The specimens for corrosion tests were prepared by the same procedure as described for nonoxide ceramics in the Part I of this paper.<sup>1</sup> Rectangular bars 3 mm × 4 mm × 50 mm were cut, ground, and the tensile faces polished up to 6 μm. Before immersion in corrosive medium the samples were ultrasonically cleaned in acetone for 15 min, rinsed with distilled water, and put into a cabinet dryer for 3 h at 110°C. The stainless-steel PTFE-lined pressure reactors were used for the corrosion tests both under static and quasi-dynamic conditions.

N. Jacobson—contributing editor

Manuscript No. 28728. Received October 6, 2010; approved February 17, 2011.

This work was financially supported by the APVV grant No. APVV 0171-06 and by the grant of the Slovak Scientific Grant Agency VEGA under the contract number VEGA 2/0036/10.

\*Member, The American Ceramic Society.

†Author to whom correspondence should be addressed. e-mail: galuskova@tnuni.sk

## (2) Corrosion Experiments

In order to study the mechanisms of dissolution of the oxide ceramic materials, the conditions of the corrosion tests identical to those carried out with nonoxide ceramics were employed.<sup>1</sup> The bars were placed in PTFE-lined pressure corrosion reactors with the inside volume 26 cm<sup>3</sup> filled with corrosive liquid, deionized water (conductivity  $25 \pm 5 \cdot 10^{-4}$  S/m), or 0.5 mol/L NaCl solution and heated in laboratory drying oven. Both static and *quasi*-dynamic tests were carried out at the temperature of 290°C with maximum duration of the test 480 h. Additional static tests at temperatures 150° and 200°C were applied in order to obtain the data for determination of kinetic parameters, and for calculation of the activation energies. The ratio between the sample surface and the volume of corrosive liquid ( $S/V$ ) was held constant at  $0.7 \pm 0.03$  cm<sup>-1</sup>, i.e. two bars were placed in one reactor at the same time with 20 mL of the liquid medium. The tests were carried out in three reactors in parallel. Six specimens were tested at each condition. After the test the samples were removed from the reactors, rinsed with distilled water, dried, and weighed. In parallel, the tests without the ceramic specimens were carried out for given time interval, providing the eluate labelled as a *blank*. The concentration of the particular element detected in the *blank* was subtracted from the concentration determined in the eluates taken after the corrosion tests with the ceramic material.

## (3) Quasi-Dynamic Tests

Quasi-dynamic test conditions were also applied for determination of the kinetic parameters in case of the material AH. As a standard flow-through arrangement could not be used due to high temperatures applied, an alternative arrangement has been used, where every 22 h the reactors were cooled down, the corrosive solution was removed and fresh solution was added to the reactor. The primary aim was to avoid formation of a passivation layer due to oversaturation of the solution with respect to leached components, or at least to minimize precipitation reactions. The test was carried out at the temperature of 290°C. The  $S/V$  ratio was identical to the static tests.

## (4) Methods of Analysis

The amounts of ions dissolved in the corrosion medium were determined by inductively coupled plasma atomic emission spectroscopy (ICP-AES, Vista MPX, Varian Australia Pty Ltd., Mulgrave, Australia). The concentration of Al, Ca, and Si in the aqueous sodium chloride eluates was determined by the internal standardization technique, with beryllium as the internal standard. The amount of an element released into the solution was expressed in terms of the value  $NL_i$  in [g/m<sup>2</sup>] according to the Eqs. 1 and 2 for static and *quasi*-dynamic conditions, respectively<sup>1</sup>

$$NL_i = \frac{c_i}{w_i} \frac{S}{V} \quad (1)$$

$$NL_i' = \frac{c_i}{w_i} \frac{S}{V} + NL_i'^{-\Delta t} \quad (2)$$

where  $c_i$  is the concentration of an element (i) in solution in [mg/L],  $S$  is the surface of the ceramic material in contact with corrosive solution in [m<sup>2</sup>],  $V$  is the volume of the corrosive solution in [m<sup>3</sup>],  $w_i$  is the mass fraction of the element (i) in the ceramic material,  $t$  is the time and  $\Delta t$  is the length of the sampling interval during the *quasi*-dynamic test.

Corroded surfaces and cross sections of corroded specimens were examined by scanning electron microscopy (SEM EDX, Carl Zeiss SMT, GmbH, Jena, Germany, EVO 40 HV, accelerating beam voltage 20 kV). Before the SEM analysis the specimens were coated with gold. The phase composition of corrosion products formed at the exposed surface was

investigated with the use of X-ray diffractometer (XRD, Bruker D8 DISCOVER, Bruker AXS Inc., Madison, WI) specially designed for measurement of thin layers, in the  $2\theta$  interval 20°–80° using  $\text{CuK}\alpha$  radiation.

## III. Results

### (1) Microstructure

The microstructure of the high purity SSS alumina, the material A consists mostly of equiaxed grains with diameter of about 0.5  $\mu\text{m}$  (Fig. 1(a)) and residual porosity of only 0.2%. Pores are smaller and less frequent comparing to the microstructure of the material AH (Fig. 1(b)). The microstructure of the material AH mostly consists of the matrix of fine equiaxed alumina grains with diameter  $< 1 \mu\text{m}$  and with residual porosity 0.8%. Occasionally, a large platelet-shaped grains with the length of several tens of micrometers were present, which document that abnormal grain growth was active under the conditions of hot pressing. This is believed to be the result of local melt formation due to inhomogeneous distribution of dopants/impurities in the material.<sup>8</sup> Detailed microstructure characterization of the material AH published elsewhere<sup>9</sup> revealed the presence of approximately 0.5 nm thick amorphous grain-boundary film with Ca:Si atomic ratio ranging between 1:11 and 1:25. The composition of glass in triple pockets fell roughly into the anorthite and mullite phase fields and contained between 0–17 mol % of CaO, 62–77 mol % of SiO<sub>2</sub>, and 17–38 mol % of Al<sub>2</sub>O<sub>3</sub>. Crystalline anorthite was detected as the main secondary crystalline phase.

### (2) Static Experiments

(A) *Corrosion in Deionized Water:* The results of weight change determination obtained from experiments carried out in deionized water are at all studied temperatures and for both studied materials summarized in the Fig. 2. At 150° and 200°C the weight losses observed in material A were similar at both

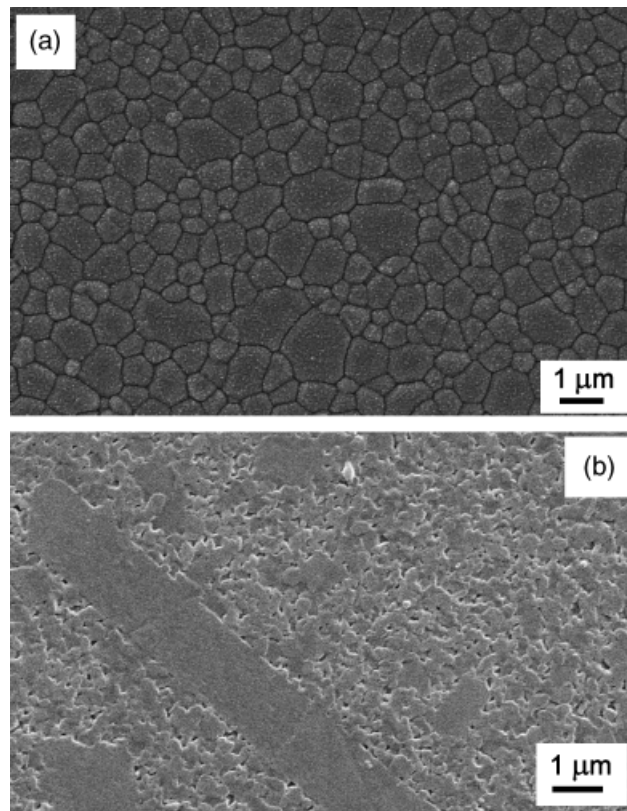
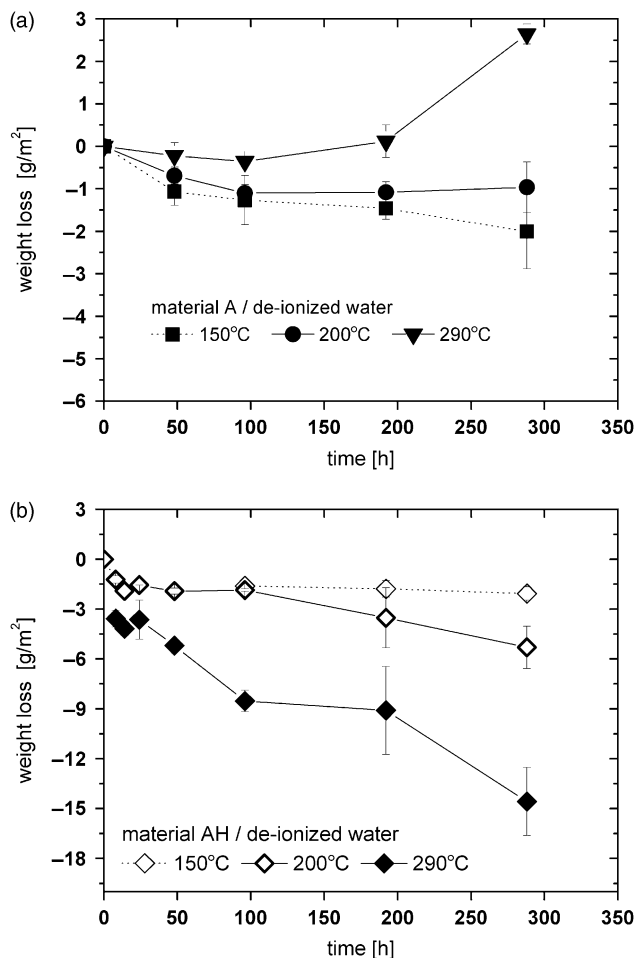


Fig. 1. Microstructure of the material A (a) and of the material AH (b).



**Fig. 2.** Weight loss as a function of time for the material A (a) and the material AH (b) corroded in deionized water.

temperatures (Fig. 2(a)) during the first 192 h. A slight weight gain was determined at 200°C for longer corrosion times. However, at 290°C notable weight gain was observed after 192 h of corrosion. The weight loss of corroded AH (LPS-alumina) specimens was temperature dependent and linear in the time interval studied. The maximum measured weight loss in AH was five times higher than in the material A (Fig. 2(b)).

The analysis of deionized water after corrosion experiments with the material A were focused on determination of aluminum as the main building element of the  $\text{Al}_2\text{O}_3$  matrix. The concentrations were recalculated to the  $NL$  values (Fig. 3(a)) according to Eq. (1) and compared with the  $NL(\text{Al})$  values obtained for the AH specimens (Fig. 3(b)). The  $NL(\text{Al})$  values in the system A were extremely low, and indicate low dissolution rate of alumina matrix. At 150°C the  $NL(\text{Al})$  values were close to the limit of detection (0.095 mg/L) of the used analytical method for aluminum, especially for short dissolution times, and are therefore not shown in the figure. The lowest but still detectable  $NL(\text{Al})$  were measured at 290°C, which corresponds to observed weight gains shown in (Fig. 2(a)), and indicates precipitation of hydrated aluminas. The  $NL(\text{Al})$  values in the system AH were systematically by one order of magnitude higher than in the system A. After initial enrichment with Al within the first 48 h of the test at 290°C a steady state was achieved.

At lower temperatures the time dependence of  $NL(\text{Al})$  goes through a maximum between 48 and 96 h of the test, after which the solution was depleted of aluminum. When evaluating the  $NL$  values in AH, the presence of the intergranular calcium aluminosilicate glassy phase must be also considered. The exact amount of aluminum incorporated into the glass containing nominally  $\text{CaO}:\text{SiO}_2$  in molar ratio 1:5 is not known, and cannot be determined due to overlapping of the electron beam with

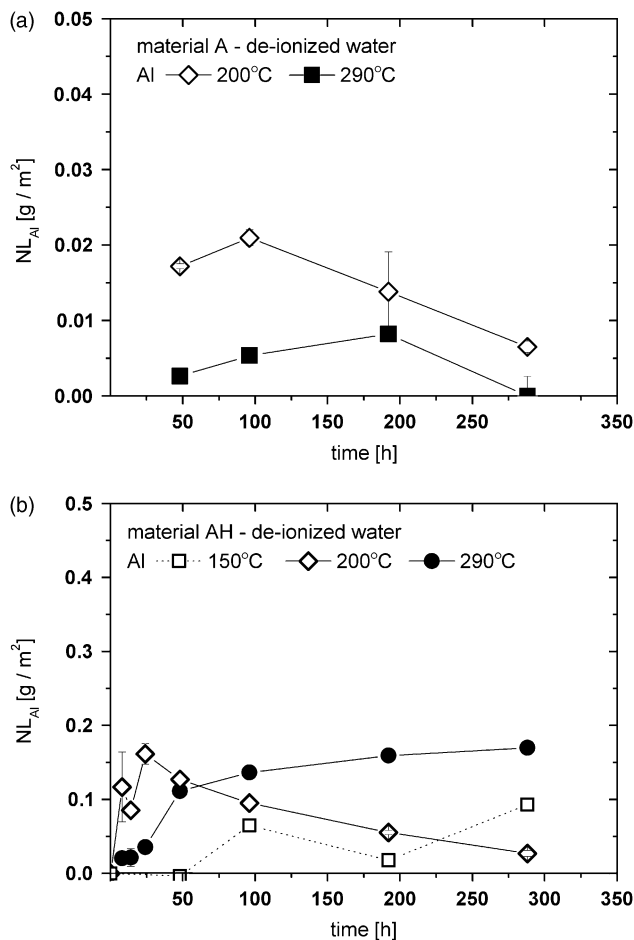


**Fig. 3.**  $NL(\text{Al})$  as a function of time for A (a) and AH (b) specimens corroded in deionized water.

neighboring alumina grains. The calculated  $NL$  values are thus normalized with respect to overall Al in the ceramic material, including both the alumina in the matrix grains and the Al in grain-boundary phase. Considering the extremely low dissolution rate of alumina matrix in the material A, the contribution of aluminum from the matrix in the eluate is also likely to be negligible in the material AH. The main source of Al is therefore the aluminosilicate grain-boundary phase with low calcia-to-silica ratio and unknown aluminum content, and the triple pocket glass of approximately anorthite composition. The  $NL(\text{Al})$  values normalized with respect to the overall Al content in the materials thus provides only strongly biased information on dissolution rate of AH. The analysis of corrosion solutions was therefore focused on determination of calcium and silicon (Fig. 4). Nearly identical  $NL(\text{Si})$  and  $NL(\text{Ca})$  values were measured at 150°C (Fig. 4(a)), indicating congruent dissolution of grain-boundary glass. Similar congruent and linear behavior was observed also at 200°C in the initial 96 h of the test, after which the solution became depleted of calcium. No calcium was detected in the eluates from the corrosion experiments at 290°C up to 288 h (Fig. 4(b)), despite the fact that the  $NL(\text{Si})$  values show approximately linear trend until steady state is achieved after 192 h of the test.

Dissolved aluminum has a distinct tendency to form hydroxy complexes. The activity of  $\text{Al}^{3+}$  ions in water is strongly influenced by pH. Below  $\text{pH} = 4.5$  the aluminum solubility increases, but in the near-neutral pH range, the total concentration of dissolved  $\text{Al}^{3+}$  becomes as low as  $1 \mu\text{mol/L}$ .<sup>10</sup> The pH values of the water leaching medium after the corrosion experiments carried out at 290°C was in the range from 6.1 to 7.1 (measured at 25°C). Based on this information we can assume that under these conditions all dissolved aluminum was present either in the

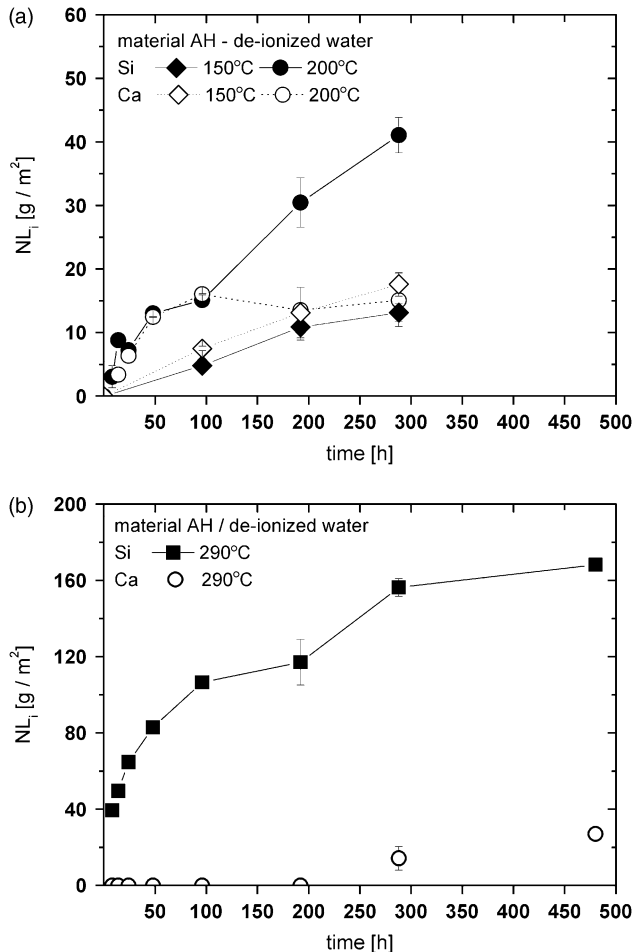


**Fig. 4.**  $NL(\text{Si})$  and  $NL(\text{Ca})$  as a function of time for the specimen AH corroded in deionized water at 150°, 200°C (a), and at 290°C (b).

form of  $\text{Al}(\text{OH})_3^0$  or as  $[\text{Al}(\text{OH})_4]^-$ ,<sup>11,12</sup> until the equilibrium was reached. The initial precipitates were likely amorphous hydroxides that could be either aged under hydrothermal conditions of the test or formed during cooling of the autoclave, to yield crystalline corrosion products. The SEM analysis of the sample A surface corroded in deionized water at 290°C for 288 h revealed the presence of significant amount of corrosion products with well-defined facets indicating their crystalline nature (Fig. 5(a)). The XRD pattern of the precipitates removed from corroded surfaces confirmed the presence of  $\text{AlOOH}$  phase in the form of boehmite (Table I). A more detailed view of the area without precipitates (Fig. 5(b)) revealed partially dissolved rounded grains of  $\alpha\text{-Al}_2\text{O}_3$  and the places where loosened corroded grains detached from the alumina matrix as the result of the corrosion process.

Dissolution of the material AH and the chemistry of the corrosion solution in the initial stage of dissolution might be influenced by the concentration of released Al ions. The results from this study at 290°C show that  $NL(\text{Si})$  increase rapidly in the first

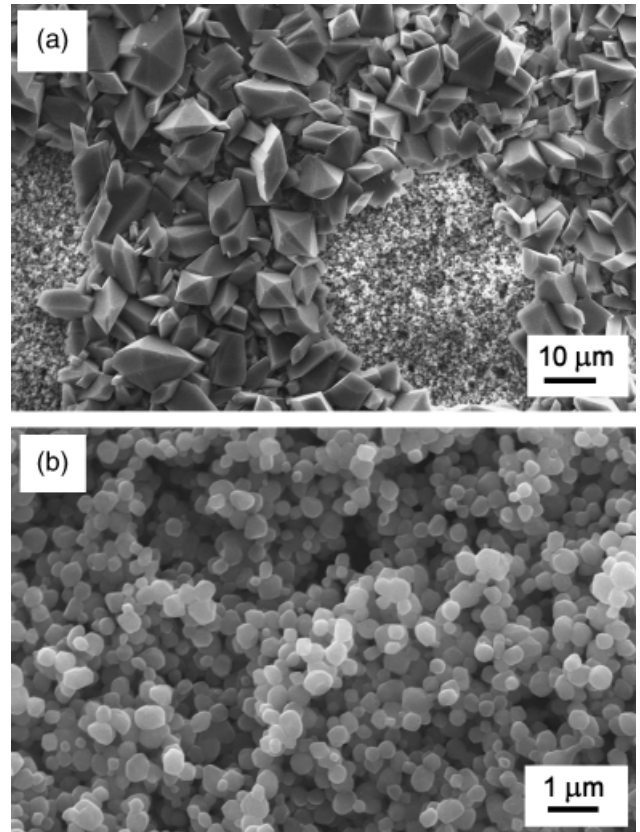


**Fig. 5.** The morphology of the specimen A corroded in deionized water for 288 h at 290°C (a) The faceted grains represent precipitated corrosion products. Detailed scan of the circular area in the right hand side of the micrograph (a) revealing partially dissolved  $\alpha$ -alumina grains (b).

48 h due to dissolution of grain-boundary glass and continue to grow in the next 480 h. At the neutral pH aluminum is likely to be present in the soluble form of  $[\text{Al}(\text{OH})_4]^-$  as the consequence of bonding the  $\text{Al}^{3+}$  ions with  $\text{OH}^-$  in later stages of dissolution when the steady state is achieved. The normalized amount of aluminum released into the solution after 24 h was 36  $\text{mg}/\text{m}^2$  and after 480 h of dissolution 300  $\text{mg}/\text{m}^2$  (Fig. 3(b)). The presence of  $\text{Al}^{3+}$  and  $\text{Si}^{4+}$  together with  $\text{Ca}^{2+}$  ions in the solution gives rise to a number of identifiable soluble/insoluble compounds. Moreover, the solution is evidently depleted of calcium. The depletion is observed after 96 h of the test at 200°C and from the beginning of the dissolution process at 290°C. The morphology of corroded surface of the specimen AH after only 8 h at 290°C (Fig. 6) revealed needle-shaped corrosion products, which differ markedly from the angular crystals found on corroded surface of the material A. The XRD of the corrosion products removed from the corroded surface after 480 h at 290°C confirmed the presence of crystalline phases of the anorthite type (anorthite and dmisteinbergerite) with the molecular formula  $\text{CaO} \cdot \text{Al}_2\text{O}_3 \cdot 2\text{SiO}_2$  (Table I), where Ca, Si incorporated in the mineral structure originated from the

**Table I.** The Crystalline Phases Identified by the X-Ray Diffraction of the Corrosion Products Removed from the Corroded Surface of the Ceramic Material after 480 h at 290°C

Specimens	X-ray analysis of the corrosion products after corrosion of the material in	
	Deionized water	0.5 mol/L NaCl
CP-A	Boehmite/ $\text{AlOOH}$ (83-2384) Corundum/ $\text{Al}_2\text{O}_3$ (71-1123)	
CP-AH	Anorthite/ $\text{CaO} \cdot \text{Al}_2\text{O}_3 \cdot 2\text{SiO}_2$ (89-1459) Dmisteinbergerite/ $(\text{CaAl}_2\text{Si}_2)\text{O}_8$ (51-64) Corundum/ $\text{Al}_2\text{O}_3$ (71-1123)	Analcime/ $\text{Na}(\text{Si}_2\text{Al})\text{O}_6$ (74-2219)

CP, corrosion products removed from the material.

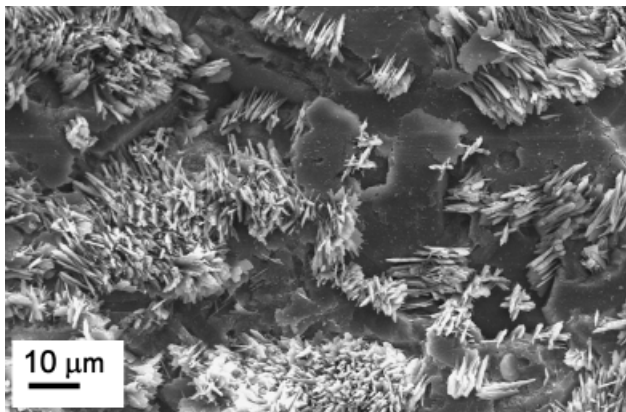


Fig. 6. SEM micrograph of the AH surface exposed to deionized water for 8 h at 290°C.

grain-boundary glass together with Al of, very likely, the same origin. The corundum phase identified in the corrosion product originates from the uncorroded material removed together with corrosion products during mechanical separation of the layer.

(B) *Corrosion in an Aqueous Sodium Chloride Solution:* Unlike for dissolution in deionized water no weight-gain was observed in the material A corroded in 0.5M NaCl solution at 290°C (Fig. 7(a)). The time-weight loss dependences differed only slightly, irrespective of the temperature. The time-weight loss dependences of the material AH showed similar linear trends at 150° and 200°C. However, at 290°C the weight decreased significantly, similar to deionized water, and approximately linearly with time up to 192 h of the test (Fig. 7(b)). The

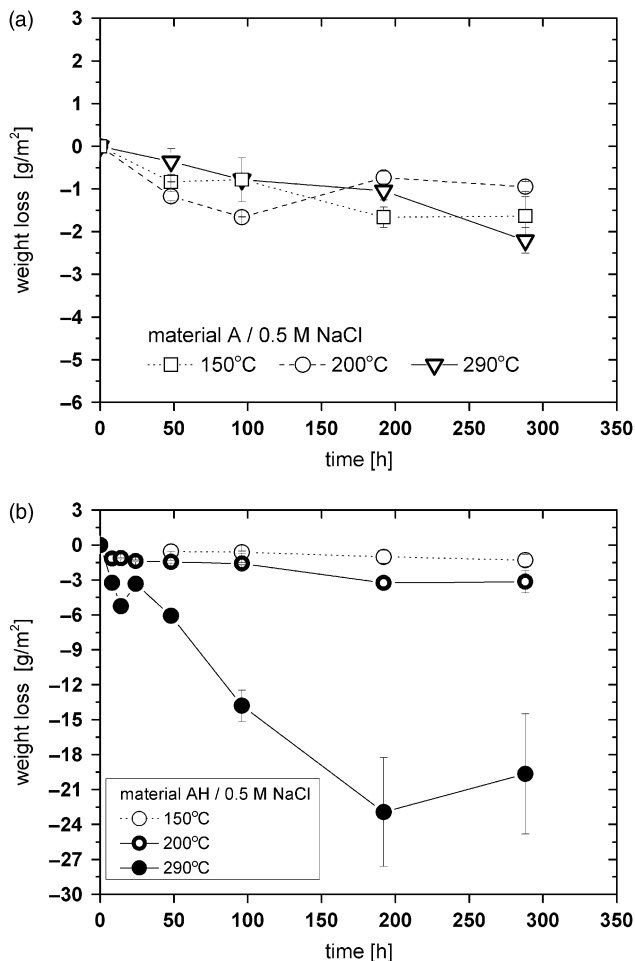


Fig. 7. Weight loss as a function of time for the material A (a) and AH (b) corroded in 0.5M NaCl solution.

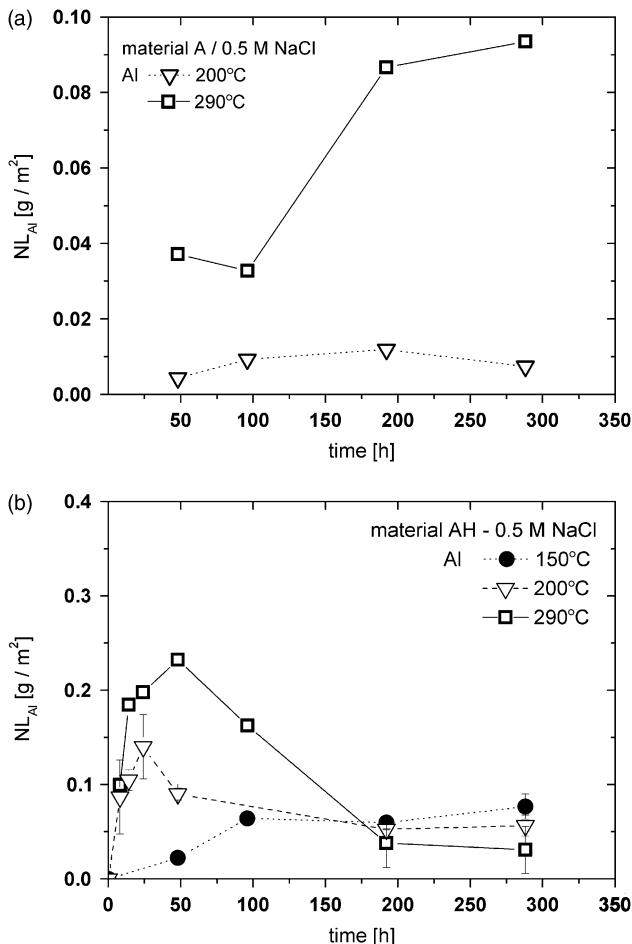


Fig. 8.  $NL(Al)$  as a function of time for A (a) and AH (b) specimens corroded in 0.5M NaCl solution.

$NL(Al)$  values in the aqueous sodium chloride solution for the material A were very low up to 200°C, but at the temperature 290°C significant increase of the  $NL(Al)$  with time was observed (Fig. 8(a)).

In the material AH the aluminum content increased rapidly, and approximately linearly, in the initial period of the test, going through a maximum of 230 mg/m<sup>2</sup> at about 48 h, and followed by possible formation of colloid Al(OH)<sub>3</sub> resulting to depletion of Al to 30 mg/m<sup>2</sup> with extension of the test over 288 h (Fig. 8(b)). The initial aqueous aluminum concentration, together with the presence of Na<sup>+</sup> ions in the NaCl solution are likely to control the Si and Ca release, as well as precipitation of Si and Ca-containing corrosion products in both aqueous solutions. Calcium precipitated in deionized water eluates, while the content of silicon increased linearly. In the NaCl solution Ca remained in soluble form even during the corrosion at 290°C (Fig. 9), while solution became gradually depleted of silicon in later stages of the material dissolution. In both corrosion solutions the concentration of Si achieved the value 200 ± 50 mg/L at 290°C, which might indicate the equilibrium concentration of silicon under the applied conditions.

The corroded surfaces of the material AH were coated with a compact crust of precipitates with scattered globular clusters with diameters ranging from 10 to 200 μm (Fig. 10). The EDX analysis confirmed the presence of Si, Al, and Na in the clusters. The crust itself consisted of fine star-like dendritic crystallites with the length of individual needles in the range from 1 to 2 μm (Fig. 10(b)). Detailed XRD analysis of the globular clusters removed from the precipitated surface confirmed the presence of analcime (Na(Si<sub>2</sub>Al)O<sub>6</sub>, PDF 74-2219) crystalline phase (Table I), in accord with the measured concentrations of leached elements, which indicated precipitation of a silicate, calcium-free phases from the NaCl solution after 196 h testing at 290°C.

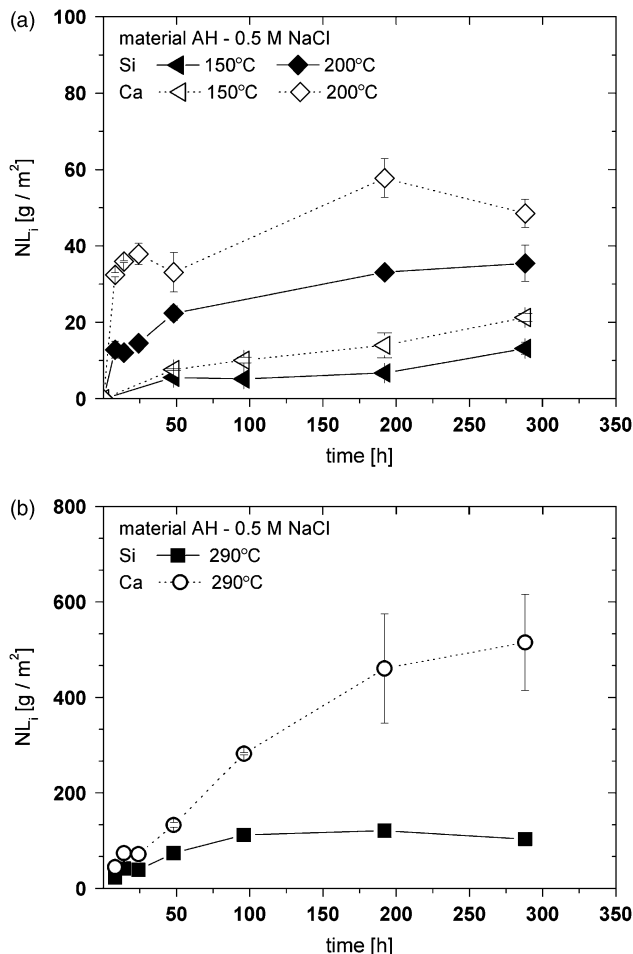


Fig. 9.  $NL(\text{Si})$  and  $NL(\text{Ca})$  as a function of time for AH specimens corroded in 0.5M NaCl at 150°, 200°C (a), and at 290°C (b).

(C) *Quasi-Dynamic Conditions:* Both corrosion solutions under static conditions at 290°C became enriched with the metal ions transferred from the dissolved material until thermodynamically stable reaction products were formed to hinder further dissolution process. In order to obtain data for determination of the initial dissolution rate of the material AH, quasi-dynamic arrangement of the experiment was used. The cumulative  $NL$  values of the leached aluminum, calcium, and silicon calculated according to the Eq. (2)<sup>1</sup> and their time dependences in deionized water and in the 0.5 mol/L NaCl solution are, respectively, shown in Figs. 11(a) and (b). The morphology of the corroded surfaces from both corrosion solutions are shown in Fig. 12.

The total concentration of calcium in deionized water eluates after subtraction of the *blank* experiment was close to zero. The concentration of Al in the eluate after each 22 h period did not exceed the average value of 3 mg/L in an early stage of the experiment, then decreased to 1 mg/L. Such decrease is explained either by the hindrance of the leaching process by the layer of precipitates or by gradual exhaustion of the surface corrosion layer with respect to the leached ions with extension of the test. Nearly identical maximal cumulative  $NL(\text{Al})$  value, 400 mg/m<sup>2</sup> was measured in both corrosion solutions. The total weight losses measured after the tests in deionized water and in the NaCl solution were respectively 0.002 (RSD 8%) and 0.004 g/cm<sup>2</sup> (RSD 29%), although these values might be influenced by the formation of new secondary phases attached to the surface of specimens. The morphology of new reaction products differed, depending on the solution. Sporadically aggregated needle-shaped crystals were observed after the tests in deionized water and the lamellas of various orientation covered the ceramic surface in contact with the NaCl solution (Fig. 12). The phase composition of the precipitates was identical to those formed

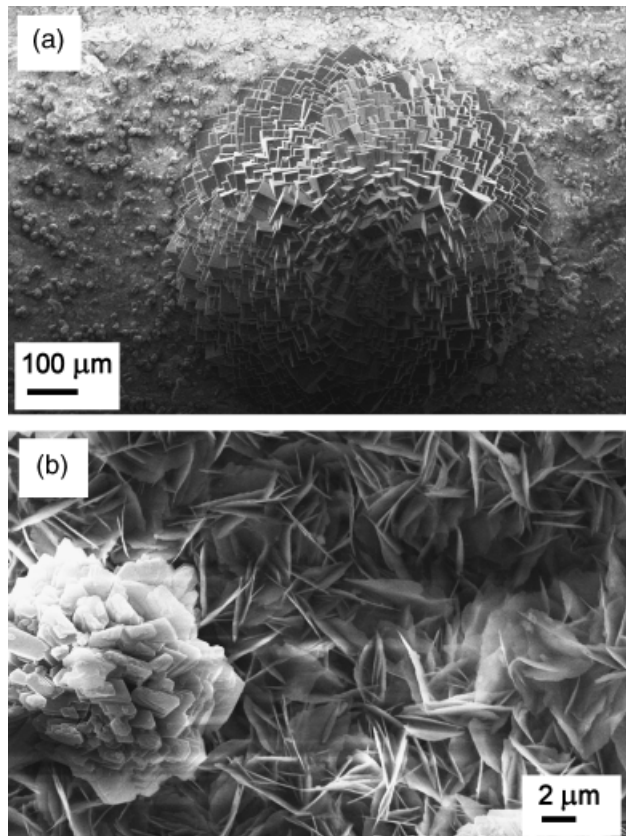


Fig. 10. SEM micrograph of the globular cluster (a) and star-like dendritic crystallites (b) on the surface of specimen AH corroded for 288 h in 0.5M NaCl at 290°C.

under static conditions, i.e. anorthite in deionized water and analcime in aqueous sodium chloride solution. Interestingly, the precipitates did not seem to cover the prismatic planes of abnormally grown alumina grains, which then remain exposed to corrosion solution (Figs. 12(a) and (b)). This effect might be related to different quality of corroded surfaces: the abnormal grains remain largely smooth and unaffected by the corrosion, preventing the formation of new phase nuclei. At the same time the boundaries in fine-grained matrix are etched, creating uneven surface facilitating nucleation and precipitation of new phases.

Apart from the precipitated layer of corrosion products the EDX analysis revealed an approximately 400 μm thick surface layer significantly depleted of calcium and silicon in specimens corroded in both media. The layer could be clearly distinguished also on SEM micrographs appearing brighter comparing to dark uncorroded core, and according to EDX analysis the content of both Ca and Si was close to detection limit of the method. The layer is characteristic also by the presence of clearly distinguishable abnormal alumina grains, which are etched from the surrounding matrix. The Ca and Si contents determined by EDX in the uncorroded area beyond the depleted layer were, respectively, 0.46 and 1.03 at.-%.

(D) *Corrosion Rates and Activation Energies:* As shown by the results of the static tests, dissolution of the specimen A is influenced by the temperature. Moreover, aluminum released from the studied material has strong tendency to create complex ions or to be incorporated into the corrosion products attached to the specimen surfaces, especially those corroded at 290°C. The rate constants of dissolution at 150°C for the material A could not be determined as the concentrations of aluminum in eluates were close to the limit of detection. Also determination of the activation energies of dissolution of the material A from only two allowable kinetic parameters would be rather questionable, and are therefore not considered.

Dissolution processes of the material AH were evidently influenced by the temperature of the corrosion media. The rate

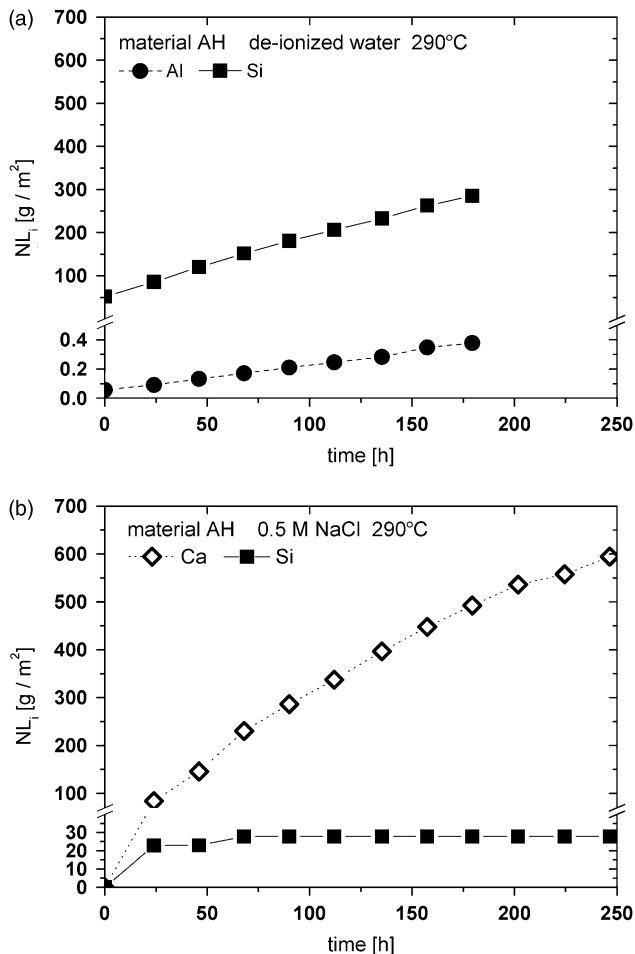


Fig. 11. Time dependences of  $NL(\text{Al}, \text{Ca}, \text{Si})$  leached from the specimen AH in deionized water (a) and in aqueous sodium chloride solution (b).

constants of dissolution at the two temperatures lower than 290°C and also at 290°C were determined from the linear parts of the experimental  $NL$  (mol/m<sup>2</sup>) versus time dependences obtained from the analysis of the data acquired, respectively, from static and *quasi*-dynamic tests. Additionally, calculations of the rate constants were based on the element which was not incorporated to the secondary phases formed due to oversaturation of the solution, i.e. Si and Ca in deionized water (Figs. 4(a) and 11(a)) and NaCl solution (Figs. 9(a) and 11(b)), respectively. Experimentally, the activation energies were obtained from the slope of a plot  $\ln k$  vs.  $1/T$  using the Arrhenius equation

$$\ln k = \ln A - E_a/(RT) \quad (3)$$

The values of rate constants and the activation energies for both studied ceramic materials are summarized in Table II.

The rate constants of dissolution of the material A were almost three orders of magnitude lower than the rate constants of the material AH. The apparent activation energy of dissolution of the AH ceramic material in deionized water and in 0.5M NaCl solution was  $48.3 \pm 0.6$  and  $49.0 \pm 0.1$  kJ/mol, respectively. The value of the activation energies reported for dissolution of alumina ceramics with purity 99.8% corroded by various acids was determined to be 10.68 kJ/mol in HCl and 9.74 kJ/mol in H<sub>2</sub>SO<sub>4</sub>.<sup>6</sup> Mikeska and Bennison<sup>3</sup> determined the activation energies for alumina samples codoped with MgO and SiO<sub>2</sub> dissolved in aqueous hydrofluoric acid in the range of 30–90 kJ/mol depending on composition of the grain-boundary glassy phase. They conclude that low activation energies, at the level of 30 kJ/mol in silica-doped aluminas is close to that of dissolution of SiO<sub>4</sub> tetrahedra, while high activation energies characteristic for aluminas with Mg/Si ratio  $\geq 1$  are similar to those of dissolution

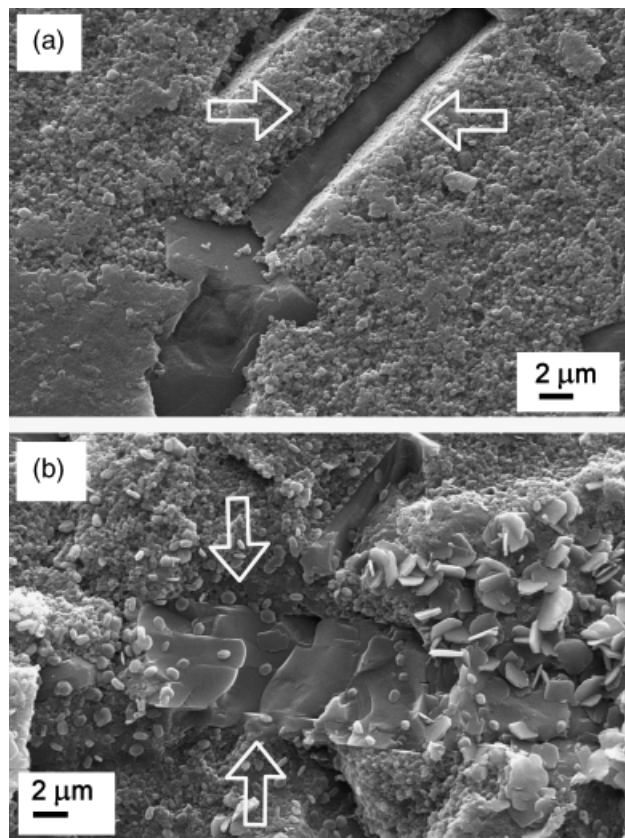


Fig. 12. SEM micrograph of the specimen AH analyzed after corrosion in deionized water (a) and in aqueous sodium chloride solution (b) under *quasi*-dynamic conditions at 290°C. The exposed prismatic planes are marked with arrows.

of AlO<sub>6</sub> octahedra (102 kJ/mol). Therefore, the mechanism of dissolution of silica-doped aluminas in HF is the same that of the fused silica, while the mechanism of dissolution MgO codoped materials with higher than equimolar Mg/Si ratio is similar to pure sapphire. The values of activation energies obtained in this study for the material AH with Ca/Si ratio 0.2 therefore confirm the results of chemical analysis of eluates, i.e. that the material corrodes by preferential dissolution of the aluminosilicate grain-boundary phase, or, more specifically by congruent dissolution of the aluminosilicate network with simultaneous release of Ca<sup>2+</sup> ions.

#### IV. Discussion

It is generally accepted that the corrosion resistance of alumina ceramics is closely related to their purity.<sup>2,3,13,14</sup> Even for high-purity alumina, attack can occur at grain boundaries where small amounts of silica-based impurities segregate and are preferentially dissolved by aqueous fluids.  $\alpha$ -alumina crystals have dense structure where aluminum-oxygen octahedra form an interpenetrating lattice with strong interatomic bonds, which makes the corrosion attack particularly difficult. Detailed insight in SEM micrographs of the material A corroded at 290°C (Fig. 5(b)), revealed that all Al<sub>2</sub>O<sub>3</sub> matrix grains at the surface had round edges and in some places the grains have been detached from the material. It cannot be excluded that some of Al<sub>2</sub>O<sub>3</sub> grains were detached due to preferential decomposition of small amounts of Si-impurities segregated at the grain boundaries. Dissolution of grains themselves could be assigned to possible metal-proton exchange reactions, the reversible exchange of OH<sup>-</sup> for Al, yielding [Al(OH)<sub>4</sub>]<sup>-</sup>. The increase of temperature up to 290°C greatly influences speciation of Al in solution, resulting in precipitation of new secondary phases. Alumina has been shown by Sato *et al.*<sup>5</sup> to dissolve in aqueous solution at 150–200°C containing NaOH by the following reactions:

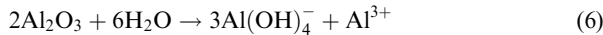
**Table II.** The Activation Energies of Dissolution of the Material AH, and Rate Constants Measured for Corrosion in Deionized Water and in 0.5M NaCl Solution

Specimen	Deionized water		0.5 mol/L NaCl	
	$k$ mmol(m <sup>2</sup> ·h) <sup>-1</sup>	$E$ [kJ/mol]	$k$ mmol(m <sup>2</sup> ·h) <sup>-1</sup>	$E$ [kJ/mol]
Material A				
290°C	0.0021 ± 0.0001	— <sup>†</sup>	0.014 ± 0.001	— <sup>†</sup>
200°C	0.009 ± 0.001		0.0026 ± 0.0003	
150°C	—		—	
Material AH				
290°C	50 ± 1	48.3 ± 0.6	67 ± 2	49.0 ± 0.1
200°C	5.4 ± 0.4		9.7 ± 3	
150°C	1.7 ± 0.1		2.1 ± 0.3	

<sup>†</sup>Not determined.



with the second reaction being the faster of the two. According to phase distribution diagram, the principal Al specie in the presence of OH<sup>-</sup> is the aluminate ion [Al(OH)<sub>4</sub>]<sup>-</sup>.<sup>12</sup> As our experiments were carried out in the solutions with neutral pH, amorphous Al(OH)<sub>3</sub> precipitates can also form along with the aluminate ions: these can be hydrothermally aged to yield crystalline products. Speaking in terms of Al speciation, the pH value 6.9 ± 0.3 determined in deionized water after the corrosion tests falls into the neutral solution range. The dissolution equation (Eq. (6)) is then proposed to proceed as follows:



Precipitation of Al<sup>3+</sup> ions in the form of boehmite (AlOOH), as the new secondary phase covering the surface of the specimen A corroded in deionized water, was detected by various analytical techniques. Summarizing the weight loss measurements and the solution chemistry, the corrosion of the specimen A in both corrosion solutions comprised the mentioned dissolution process with partial precipitation of aluminum hydroxid-oxides. However, the process was rather slow when comparing to dissolution of the material AH.

The hypothesis that corrosion of the AH ceramics proceeds via dissolution of the grain-boundary glassy phase is supported by the eluate chemistry together with the analysis of corroded surfaces and newly formed secondary phases. The mechanism of dissolution reported for aluminosilicate oxides and glasses can be therefore applied, as the presence of calcium aluminosilicate glass phase was confirmed at the grain boundaries.<sup>9</sup> Jantzen *et al.*<sup>15</sup> treats dissolution of such glasses through activated complex as a rapid removal of univalent and divalent cations from the near surface by ion exchange followed by the slower exchange of Al<sup>3+</sup> for 3H<sup>+</sup> protons in solution. Divalent metal-oxygen bonds break faster than trivalent metal-oxygen bonds, which break faster than Si-O bonds.<sup>16</sup> The Al<sup>3+</sup>-proton exchange does not destroy the glass framework but it partially liberates three adjoining silica tetrahedra to which it is bonded. It is the detachment of the partially liberated silica that is the rate-determining step, that is, partially detached silica dissolves more readily than bonded or “attached” tetrahedral silica.

After Ca, Al, and Si are released from the grain-boundary glass of the attacked ceramic material, various reactions can occur due to the complex solution chemistry. The hydrolysis of Al(III) is characterized by a series of mononuclear as well as polynuclear species. It has been shown that [Al(OH)<sub>2</sub>]<sup>3+</sup> undergoes successive deprotonation steps to yield [Al(OH)]<sup>2+</sup>, [Al(OH)<sub>2</sub>]<sup>+</sup>, and Al(OH)<sub>3(aq)</sub>.<sup>17</sup> In neutral solution and upon increasing pH the amorphous Al(OH)<sub>3(aq)</sub> dissolves and the aluminate ion, [Al(OH)<sub>4</sub>]<sup>-</sup> is formed.<sup>17</sup> Dissolved Si(IV) specie is mostly Si(OH)<sub>4</sub>. It is a weak acid, of which the first degree dissociation produces H<sub>3</sub>SiO<sub>4</sub><sup>-</sup> and H<sup>+</sup> at a pH < 9, and at higher

pH, Si(OH)<sub>4</sub> further dissociates into H<sub>2</sub>SiO<sub>4</sub><sup>2-</sup>/HSiO<sub>3</sub><sup>3-</sup>/SiO<sub>4</sub><sup>4-</sup> and produces more H<sup>+</sup>.<sup>18,19</sup> In the presence of [Al(OH)<sub>4</sub>]<sup>-</sup>, Ca<sup>2+</sup>, and Si(OH)<sub>4</sub> various complexes such as Al(OH)<sub>3</sub>H<sub>3</sub>SiO<sub>4</sub> can be formed along with other corrosion products, e.g. anorthite (CaO·Al<sub>2</sub>O<sub>3</sub>·2SiO<sub>2</sub>) confirmed by XRD at the surface of AH corroded in deionized water. In the contrary, in aqueous environment with Na<sup>+</sup> ions, analcime (Na(Si<sub>2</sub>Al)O<sub>6</sub>) was identified as the main reaction product (Table I), while calcium remained in a soluble form. Calcium together with silicon were not detected with EDX analysis in the corrosion affected, approximately 400 μm thick, layer. Similar dissolution rate constants were acquired for deionized water and the NaCl solution.

## V. Conclusion

### (1) Static Conditions

Dissolution in both corrosion media of the material A was found to be an extremely slow, temperature-dependent process. Partial dissolution of alumina matrix grains was documented by rounding of the surface grain edges. Loosening and detachment of some matrix grains explained by grain-boundary attack and possible dissolution of small amounts of silicon-containing grain boundary segregated impurities is considered as the principal mechanism of material degradation. Hydroxylaluminates, identified by XRD as boehmite, precipitate to form the discontinuous layer at the surface of the specimens corroded at 290°C in deionized water.

Corrosion of the material AH is by three orders of magnitude faster than that of the material A, and attacks preferentially the calcium aluminosilicate grain-boundary glass. The initial dissolution rates of 50 and 67 mmol(m<sup>2</sup>·h)<sup>-1</sup> were determined at the temperature 290°C in deionized water and in the aqueous sodium chloride solution, respectively. The apparent activation energies 48.3 ± 0.6 kJ/mol (*deionized water*) and 49.0 ± 0.1 kJ/mol (*NaCl solution*) suggest metal-proton exchange reactions and dissolution of SiO<sub>4</sub> tetrahedra as the rate-controlling dissolution mechanism. In deionized water saturation of the corrosion solution was observed, accompanied by precipitation of anorthite-type compounds, and by significant depletion of the corrosion solution of Ca. In the aqueous sodium chloride solution analcime, Na(Si<sub>2</sub>Al)O<sub>6</sub>, was detected by XRD as the main precipitated phase after 480 h of corrosion. Precipitation of analcime was accompanied by depletion of the eluate of Si.

### (2) Quasi-Dynamic Conditions

The *quasi-dynamic* conditions applied during the tests were not able to prevent completely the attainment of the equilibrium resulting in precipitation of secondary phases and partially covering the surfaces of corroded specimens. Needle-like precipitates of anorthite assembled to spherical aggregates were found at surfaces corroded in deionized water and the lamellas aggregated to globular clusters of analcime were observed at the surfaces of the material AH exposed to the aqueous sodium

chloride solution. Irrespective to the corrosion solution used no precipitation was observed at prismatic plates of abnormally grown alumina grains, which remained exposed to corrosion media. The surface leached layer with the thickness up to 400  $\mu\text{m}$  was nearly depleted of Ca and Si, as confirmed by the EDX analysing.

### Acknowledgments

This publication was created in the frame of the project "Centre of excellence for ceramics, glass, and silicate materials" ITMS code 262 201 20056, based on the Operational Program Research and Development funded from the European Fund of Regional Development. The authors also wish to express their thanks to Dr. Robert Klement for helpful discussions.

### References

- <sup>1</sup>D. Galusková, M. Hnatko, D. Galusek, and P. Šajgalík, "Corrosion of Structural Ceramics under Sub-critical Conditions in Aqueous Sodium Chloride Solution: Dissolution of  $\text{Si}_3\text{N}_4$ -based Ceramics Part I," *J. Am. Ceram. Soc.* (in press) (2011).
- <sup>2</sup>M. Schacht, N. Boukis, and E. Dinjus, "Corrosion of Alumina Ceramics in Acidic Aqueous Solutions at High Temperatures and Pressures," *J. Mater. Sci.*, **35**, 6251–8 (2000).
- <sup>3</sup>K. R. Mikeska and S. J. Bennison, "Corrosion of Alumina in Aqueous Hydrofluoric Acid," *J. Am. Ceram. Soc.*, **82** [12] 3561–6 (1999).
- <sup>4</sup>W. Genthe and H. Hausner, "Influence of Chemical Composition on the Corrosion of Alumina in Acids and Caustic Solutions," *J. Eur. Ceram. Soc.*, **9**, 417–25 (1992).
- <sup>5</sup>T. Sato, S. Sato, and A. Okuwaki, "Corrosion Behavior of Alumina Ceramics in Caustic Alkaline Solutions at High Temperatures," *J. Am. Ceram. Soc.*, **74** [12] 3081–4 (1991).
- <sup>6</sup>L. Curkovic, M. F. Jelača, and S. Kurajica, "Corrosion Behaviour of Alumina Ceramics in Aqueous HCl and  $\text{H}_2\text{SO}_4$  Solutions," *Corr. Sci.*, **50**, 872–8 (2008).

<sup>7</sup>P. Kritzer, N. Boukis, and E. Dinjus, "Factors Controlling Corrosion in High-Temperature Aqueous Solutions: A Contribution to the Dissociation and Stability Data Influencing Corrosion Processes," *J. Supercrit. Fluids*, **15**, 205–27 (1999).

<sup>8</sup>I. J. Bae and S. Baik, "Abnormal Grain Growth in Alumina," *J. Am. Ceram. Soc.*, **80**, 1149–56 (1997).

<sup>9</sup>P. Švančárek, D. Galusek, F. Loughran, A. Brown, R. Brydson, A. Atkinson, and F. Riley, "Microstructure-Stress Relationships in Liquid Phase Sintered Alumina Modified by the Addition of 5 Weight % of Calcium-Silica Additives," *Acta Mater.*, **54**, 4853–63 (2006).

<sup>10</sup>C. A. J. Appelo and D. Postma, *Geochemistry, Groundwater and Pollution*, 2nd edition, pp. 381–2. A.A. Balkema Publishers, Leiden, 2005.

<sup>11</sup>S. Castet, J. L. Dandurand, J. Schott, and R. Gout, "Boehmite Solubility and Aqueous Aluminum Speciation in Hydrothermal Solutions (90–350°C): Experimental Study and Modeling," *Geochim. Cosmochim. Acta*, **57**, 4869–84 (1993).

<sup>12</sup>N. Moller, Ch. Christov, and J. Weare, "Thermodynamic Models of Aluminium Silicate Mineral Solubility for Application to Enhanced Geothermal Systems", *Proceedings: Thirsty-First Workshop on Geothermal Reservoir Engineering*, SGP-TR-179, Stanford University, Stanford, CA, January 30–February 1, 2006.

<sup>13</sup>K. Oda and T. Yoshio, "Hydrothermal Corrosion of Alumina Ceramics," *J. Am. Ceram. Soc.*, **80** [12] 3233–6 (1997).

<sup>14</sup>N. Boukis, N. Claussen, K. Ebert, R. Janssen, and M. Schacht, "Corrosion Screening Tests of High-Performance Ceramics in Supercritical Water Containing Oxygen and Hydrochloric Acid," *J. Eur. Ceram. Soc.*, **17**, 71–6 (1996).

<sup>15</sup>C. M. Jantzen, K. G. Brown, and J. B. Pickett, "Durable Glass for Thousands of Years," *Inter. J. Appl. Glass Sci.*, **1** [1] 38–62 (2010).

<sup>16</sup>J. Schott, O. S. Pokrovsky, and E. H. Oelkers, "The Link Between Mineral Dissolution/Precipitation Kinetics and Solution Chemistry," *Rev. Mineral. Geochem.*, **70**, 207–58 (2009).

<sup>17</sup>L. Spadini, P. W. Schindler, and S. Sjöberg, "On the Stability of the  $\text{AlOSi}(\text{OH})_3^+$  Complex in Aqueous Solution," *Aquat. Geochem.*, **11**, 21–31 (2005).

<sup>18</sup>R. K. Iler, "Effect of Adsorbed Alumina on Solubility of Amorphous Silica in Water," *J. Colloid Inter. Sci.*, **43**, 2399–408 (1973).

<sup>19</sup>F. J. Hingston and M. Raupach, "Reaction Between Monosilicic Acid and Aluminium Hydroxide. I. Kinetics of Adsorption of Silicic Acid by Aluminium Hydroxide," *Aust. J. Soil Res.*, **5** [2] 295–309 (1967). □